EXPERIMENTAL AND MODELING STUDY OF THE OXIDATION OF FENCHONE, A HIGH-ENERGY DENSITY FUEL-ADDITIVE

L Boualem, Z Serinyel, A Nicolle, M Lailliau, P Dagaut, G Dayma

EXPERIMENTAL AND MODELING STUDY OF THE OXIDATION OF FENCHONE, A HIGH-ENERGY DENSITY FUEL-ADDITIVE

L. Boualem*, **, Z. Serinyel*, **, A. Nicolle*, M. Lailliau*, **, P. Dagaut** and G. Dayma*, ****

guillaume.dayma@cnrs-orleans.fr

*Université d'Orléans, Château de la Source, avenue du Parc Floral, 45067 Orléans, France

**ICARE–CNRS, 1c avenue de la recherche scientifique, 45071 Orléans, France

***Aramco Fuel Research Center, 232 avenue Napoleon Bonaparte, 92852 Rueil-Malmaison, France

Abstract

Increasing fuel energy density constitutes a potential way to reduce engine exhaust carbon emission. Fenchone, a strained ring molecule, is an interesting candidate. The present study investigates the oxidation of fenchone in a jet-stirred reactor at high pressure (10 atm) between 700 and 1180 K at constant fuel mole fraction and constant residence time of 0.1% and 0.7s, respectively. Mole fraction profiles were obtained through sonic probe sampling, and analyzed by gas chromatography and Fourier transform infrared spectrometry. More than 30 species were identified and most of them were quantified. Also, a kinetic mechanism was developed in this study and tested against the present experimental conditions showing good agreement. The present mechanism allows illuminating the major reaction pathways involved in the decomposition routes of the fuel and its primary radicals as well as the formation pathways of the quantified intermediate species. During fenchone oxidation, the carbonyl group is mostly concerted into CO, CO_2 and formaldehyde while higher carbonyl species were identified at much lower levels of concentration, indicating that decarbonylation occurs early during the oxidation process. Aromatic compounds such as benzene and toluene are formed especially in fuel-rich conditions and potential oxygenated pollutants such as methacrolein and acetaldehyde were also quantified.

1. Introduction

Reformulation of transportation fuels through the incorporation of low-carbon blendstocks such as electrofuels constitutes an important option to address the pressing climate challenges [1]. The potential use of blendstocks and additives requires an in-depth knowledge of the combustion kinetics of the emerging components as well as of the nature and quantity of pollutants formed during their oxidation and thermal decomposition.

Strained ring hydrocarbons (SRH) are of interest as high-energy density components in transportation systems. SRH are readily produced from renewable feedstocks [2]. However, the impact of SRH on soot characteristics remains unclear [3], the respective importance of cyclopentadiene, fulvene and other benzene production routes being strongly dependent on combustion conditions [4]. Abdrabou et al. [5] showed that norbornane addition to a Diesel fuel leads to a threshold soot index reduction and soot disorder increase, as a result of five-membered ring incorporation in the molecular structure of soot [6, 7]. Functionalizing SRH with oxygen-containing groups, such as alcohols or ketones, may help to further reduce SRH sooting propensity [8]. However, this would be at the expense of the SRH calorific value. In a recent study by Morajkar et al. [9], the effect of the addition of solid camphor and camphor oil to Diesel fuel on its sooting propensity is studied using a diffusion flame. The authors reported

physicochemical changes such as a smaller particle diameter in the presence of camphor, which they linked to the increased oxidative reactivity.

Up to now, combustion characteristics of the SRH have been insufficiently characterized. Among these hydrocarbons, JP-10 (mostly endo-tetrahydrodicyclopentadiene), produced by the catalytic hydrogenation of dicyclopentadiene, is probably the most studied one; e.g. [4, 10-12]. The aim of the present work is to study experimentally the combustion mechanism of fenchone (1,3,3-trimethyl-bicycloheptan-2-one), a monoterpenoid present in fennel oil, and to provide a predictive oxygenated pollutant formation model for SRH combustion, opening up the use of such SRH in specific transport applications. The only combustion-related study on fenchone goes back to 2014. That paper reports the laminar flame speeds of fenchone at 453 K [13]. The results suggest that the laminar flame speeds of fenchone in the lean side are close to those of JP-10 previously measured by Parsinejad et al. [12], and very close to those of α-pinene [14]. To the best of our knowledge, except flash pyrolysis experiments performed in the 1960's [15], there are no oxidation or pyrolysis studies reporting intermediate species, hence none providing details on fenchone decomposition routes.

The molecular structure of fenchone is illustrated in Figure 1. Among the high-density hydrocarbon fuels, structural similarities can be drawn between fenchone and norbornane (as well as 2-ethylnorbornane) for which a limited number of theoretical studies exists. For example, recently Wang et al. [16] calculated the bond energies of 2-ethylnorbornane, norbornadiene and quadricyclane at the CCSD(T)/cc-PVTZ//B3LYP/6-311++g(d,p) level of theory. According to their calculations and based on similarities, F2 is the least likely radical to be formed with a C–H bond energy around 107 kcal/mol followed by F1 with a C–H bond energy of 104–105 kcal/mol. On the other hand, C–H bonds at positions F5–F6 and F3–F4 have C–H bond energies quite similar to primary and secondary C–H bonds in alkanes.

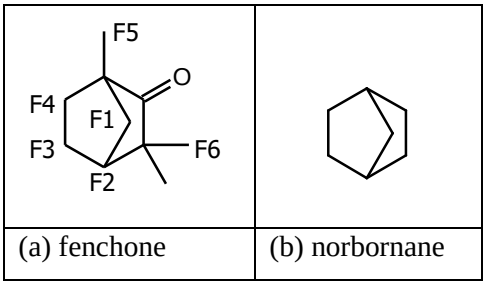

Figure 1. Structure of fenchone and radical location in F# species (a), structure of norbornane(b)

Sirjean and co-workers [17] used ab initio methods to calculate some important reaction rate constants for the decomposition of norbornane, at the CBS-QB3 level of theory. Given that there are no theoretical studies in the literature on fenchone oxidation and ab initio rate constant calculation was outside of the scope of the present study, structure/reactivity analogies were made for the mechanism development (see Section 3).

In the present study, oxidation experiments of dilute fenchone/O_2/N_2 mixtures were carried out in a jet-stirred reactor at equivalence ratios of 0.5–2 and at 10 atm, between 700 and 1180 K, with an initial mole fraction of fenchone of 1000 ppm. Reactants, products and stable intermediate species were measured and quantified. A kinetic mechanism was developed in order to describe the oxidation pathways of fenchone.

2. Experimental set-up

The present experiments were performed in a jet-stirred reactor, described in detail elsewhere [18]. The reactor is a 4 cm diameter fused-silica sphere (42 cm^3) with four injectors (nozzles of 1 mm I.D). This apparatus has been designed to provide good homogeneity under the present conditions. An HPLC pump (LC10 AD VP) with an online degasser (Shimadzu DGU-20 A3) was used to inject 1000 ppm of fenchone (>99% pure from Aldrich, L-fenchone was used) into the reactor. The fuel is pushed towards the reaction sphere with an auxiliary N_2 flow and meets the O_2/N_2 primary flows just before the JSR injectors to avoid premature fuel oxidation. The gas flow rates were controlled by mass flow controllers (Brooks). The whole injection assembly is maintained at a temperature higher than the boiling point of the fuel (467 K) to facilitate the fuel evaporation. A probe coupled with a thermocouple (0.1 mm Pt-Pt/Rh-10%), inserted into a thin-walled fused silica tube to avoid any catalytic reactions on the metallic wires, allows sampling at each desired temperature. To ensure the homogeneity of the mixture, the probe can be moved along the vertical axis of the reactor. Temperature gradient was measured to be less than 2 K cm^{-1}.

At each selected temperature, the reaction mixture was sampled using a low-pressure fused silica sonic probe. The samples were sent to analysers through a heated Teflon line maintained at 160°C. These samples were analysed using a Thermo Nexus 670 spectrometer (10 m path length, resolution 0.5 cm^{-1}, 200 mbar in the cell). The gas samples can also be stored at low-pressure in Pyrex bulbs for off-line gas chromatography analysis. Two types of detectors were used. A TCD detector coupled to a CP-Carboplot-P7 capillary column allows the quantification of O_2. FID detectors were used to measure hydrocarbons and oxygenated compounds (CP-Al_2O_3-KCl column and a CP-SIL 5CB coupled to DB1 column in two Shimadzu GC-MS 2010 Plus). Both chromatographs are coupled to a quadrupole mass spectrometer operating with electron impact ionization (70 eV) for product identification.

The species quantified in this study are end products and stables intermediates. H_2, CH_4, C_2H_4, C_2H_6, C_3H_6, allene, propyne, isoprene, methyl cyclopentadienes, benzene, and toluene were measured by gas chromatography. Few other oxygenated species were also quantified including fenchone, acetone, acetaldehyde, acrolein, methacrolein, and methyl vinyl ketone. H_2O, CO, CO_2, CH_2O were measured online by FTIR. The carbon balance was checked for each sample and found to be within ±15%. Several heavier hydrocarbons, with one or more double bonds, were separated by GC but their identification could not be achieved. According to their global formulae, using the equivalent carbon method, their mole fractions were typically < 10 ppm.

3. Kinetic mechanism

The kinetic sub-mechanism of fenchone was developed and integrated into our C_5 mechanism [19]. A list of the most important reactions is presented in Table 1. We have considered the formation of the six possible radicals even if F1 and F2 are very unlikely formed under our operating conditions due to higher C–H BDEs. This sub-mechanism was mostly developed using the RMG online database [20], but some amendments and modifications were required both in kinetic parameters and thermochemistry. As a first and simplified approach, F3 and F4 were considered as equivalent, contrary to F1, and are thus supposed to be formed at the same rate. Similarly, F5 and F6 were also both considered as equivalent, F6 being formed twice as much as F5 because of the number of available H atoms.

Table 1. The most important reactions in the fenchone sub-mechanism (units: cm^3, mol, s^{-1}, K, cal)

Reaction	A	n	Ea
H-abstraction reactions			
h+fenchone=h2+F1(1)	6.01E+03	3.02	5600.0
h+fenchone=h2+F2(11)	4.17E+03	3.02	6050.0
h+fenchone=h2+F3(5)	1.92E+09	1.50	5750.0
h+fenchone=h2+F4(3)	1.92E+09	1.50	5750.0
h+fenchone=h2+F5(9)	6.66E+05	2.54	6756.0
h+fenchone=h2+F6(7)	1.33E+06	2.54	6756.0
o+fenchone=oh+F1(1)	1.11E+03	3.19	14117.0
o+fenchone=oh+F2(11)	3.83E+05	2.41	14800.0
o+fenchone=oh+F3(5)	1.11E+03	3.19	14117.0
o+fenchone=oh+F4(3)	1.11E+03	3.19	14117.0
o+fenchone=oh+F5(9)	9.34E+03	3.02	5230.0
o+fenchone=oh+F6(7)	1.87E+04	3.02	5230.0
oh+fenchone=h2o+F1(1)	1.40E+07	1.60	470.9
oh+fenchone=h2o+F2(11)	6.87E+05	1.91	875.2
oh+fenchone=h2o+F3(5)	4.64E+07	1.61	-35.0
oh+fenchone=h2o+F4(3)	4.64E+07	1.61	-35.0
oh+fenchone=h2o+F5(9)	1.35E+00	3.81	-2897.0
oh+fenchone=h2o+F6(7)	2.70E+00	3.81	-2897.0
ho2+fenchone=h2o2+F1(1)	5.60E+12	0.00	17686.0
ho2+fenchone=h2o2+F2(11)	2.80E+12	0.00	16013.0
ho2+fenchone=h2o2+F3(5)	5.60E+12	0.00	17686.0
ho2+fenchone=h2o2+F4(3)	5.60E+12	0.00	17686.0
ho2+fenchone=h2o2+F5(9)	1.14E+02	3.19	16250.0
ho2+fenchone=h2o2+F6(7)	2.28E+02	3.19	16250.0
ch3+fenchone=ch4+F1(1)	7.90E-03	4.29	11036.4
ch3+fenchone=ch4+F2(11)	3.40E-03	4.29	12302.6
ch3+fenchone=ch4+F3(5)	6.48E+06	1.87	8780.0
ch3+fenchone=ch4+F4(3)	6.48E+06	1.87	8780.0
ch3+fenchone=ch4+F5(9)	6.00E+12	0.00	12620.0
ch3+fenchone=ch4+F6(7)	1.20E+13	0.00	12620.0
F1(1) sub-mech	9.38E+21	-1.36	101546.2
F1(1)=GD(1)+ch3	9.38E+21	-1.36	101546.2
F1(1)=GD(2)	1.13E+16	-0.48	30116.3
F1(1)=S(279)	4.79E+13	0.23	27452.4
F1(1)=GD(3)	3.98E+14	-0.07	30695.6
F1(1)=S(660)	6.92E+11	0.63	23984.4
GD(2)=c2h4+GD(7)	8.53E+09	0.76	17474.5
GD(3)=c2h4+GD(7)	1.66E+11	0.34	20999.6
S(660)=ic3h6co+mcptds2	4.55E+02	2.41	28294.3
S(279)=co+GD(11)	1.95E+18	-1.17	16546.1
GD(7)=ch3+GD(8)	4.74E+13	0.45	41411.6
GD(7)=GD(9)	9.35E+09	1.64	48145.3
GD(9)=co+GD(10)	7.07E+20	-2.08	31749.3
GD(11)=GD(12)	1.47E+05	2.22	56572.1
GD(12)=c2h4+GD(10)	2.09E+13	0.15	36085.3
GD(10)=c3h4-p+ic4h7v	5.97E+13	0.59	43858.5
F2 sub-mech			
F2(11)=S(703)	1.32E+37	-6.76	40216.1
F2(11)=S(224)	4.37E+17	-0.71	29066.7
F2(11)=ZS(16)	4.17E+43	-8.09	51534.7
F2(11)=ZS(19)+ch3	2.53E+11	1.39	87331.4
S(703)=ZS(20)	1.85E+11	0.80	26526.3
ZS(20)=dipco-2d4j+c3h4-p	1.60E+10	0.94	42338.7
S(224)=ZS(14)+co	3.89E+18	-1.17	16546.1
ZS(14)=ZS(15)	2.09E+09	1.53	33299.5
ZS(15)=c5h8-12d3m+ic4h7	1.14E+11	0.62	46331.7
ZS(16)=ZS(17)	7.79E+12	0.36	19164.9
ZS(17)=ZS(23)+co	3.89E+18	-1.17	16546.1
ZS(23)=c5h8-12d3m+ic4h7	1.14E+11	0.62	46331.6
F3 sub-mech			
F3(5)=ZS(1)	1.13E+12	0.7	28987.2
F3(5)=S(661)	6.98E+08	1.3	20704.0
F3(5)=ZS(2)	6.02E+08	1.4	23134.0
ZS(1)=ZS(3)	1.31E+17	-0.6	33236.0
S(661)=mcps2dt+ic3h6co	5.21E+20	-1.38	44728.0
ZS(2)=ZS(3)	2.34E+14	-0.4	27350.0
ZS(3)=ZS(5)+ch3	2.39E+12	0.6	38280.0

Reaction	A	n	Ea
ZS(3)=>c6h10-13d4m+co+c3h5-t	4.90E+13	0.4	34447.0
mcps2dt=mcptds2d+h	1.02E+04	3.0	30301.1
mcps2dt=ch2-cyc5-3d+h	1.59E+10	1.29	39235.4
F4(3) sub-mech			
F4(3)=GD(4)+ch3	1.90E+13	0.84	85829.5
F4(3)=GD(5)	1.37E+07	1.87	24946.9
F4(3)=GD(6)	4.30E+09	1.21	28900.0
F4(3)=S(376)	1.25E+16	-0.5	27100
GD(5)=ch3+GD(13)	3.83E+15	-0.4	30845.7
GD(5)=GD(14)	2.23E+10	0.6	23739.1
GD(5)=GD(15)	1.94E+14	0.1	29578.2
GD(6)=co+GD(18)	1.95E+18	-1.17	16546.1
S(376)=GD(14)	7.98E+14	-0.3	26613.8
S(376)=GD(20)	3.46E+15	0.0	12412.6
GD(15)=co+GD(16)	1.91E+14	-0.5	3582.1
GD(14)=but3m1dt+GD(17)	6.07E+14	-0.4	47535.5
GD(14)+ho2=co+c2h3coch3+but3m1dt+oh	4.50E+12	0.0	0
GD(16)=isope+ic4h7v	1.49E+11	1.30	42869.8
GD(16)+ho2=c2h3coch3+but3m1dt+oh	4.50E+12	0.00	0.0
GD(18)=GD(16)	8.81E+10	0.80	25424.5
GD(18)=GD(19)	2.36E+10	1.28	25612.7
GD(19)=isope+ic4h7v	5.93E+11	0.81	44528.9
GD(19)+ho2=ic3h5cho+but3m1dt+oh	4.50E+12	0.00	0.0
GD(20)=GD(21)+ic3h6co	1.19E+12	0.99	54033.3
GD(21)=c3h4-p+c3h5-a	4.73E+13	0.18	21897.3
F5(9) sub-mech			
F5(9)=S(306)	6.39E+19	-1.80	22481.8
F5(9)=S(33)	9.18E+11	0.36	16522.2
F5(9)=S(721)	1.10E-01	4.21	21839.3
S(33)=co+C9H15(38)	4.65E+17	-1.2	16546.1
S(306)=c2h4+S(260)	2.43E+13	0.1	27882.9
S(260)=ch3+C7H8O(583)	3.12E+12	0.5	28006.4
S(260)=S(582)	3.24E+09	1.4	28084.5
S(260)=GD(25)	2.83E+02	1.62	20154.3
C9H15(41)=C9H15(38)	2.32E+36	-8.1	15327
C9H15(38)=C9H15(392)	1.61E+07	2.06	20679.5
C9H15(392)=c2h4+GD(22)	2.09E+13	0.15	36085.2
GD(22)=c3h4-a+ic4h7v	6.66E+10	1.07	36182.5
GD(22bis)=c2h3+isope	2.57E+11	0.90	45027.9
GD(22bis)+ho2=c3h5-a+ic3h5cho+oh	4.50E+12	0.00	0.0
GD(22)+o2=ch2o+co+but3m1dt	4.60E+16	-1.39	1010.0
C9H15(41)=c3h4-a+GD(23)	5.21E+15	-0.32	55103.4
GD(23)=c2h4+ic4h7v	5.13E+10	0.97	35946.8
S(582)=co+GD(22)	1.22E+20	-2.11	27286.7
S(721)=GD(24)	2.71E+29	-4.70	24898.5
GD(24)=c2h4+GD(25)	3.76E+06	0.52	29123.5
GD(25)=S(2293)+but3m1dt	1.76E+16	0.33	40143.1
S(721)=GD(26)	1.72E+20	-2.32	11088.4
GD(26)=ic3h6co+GD(27)	2.27E+15	0.18	54272.0
GD(27)=c3h4-a+c3h5-a	8.11E+08	1.33	19163.3
F6(7) sub-mech			
F6(7)=S(32)	8.75E+18	-1.18	28947
F6(7)=S(305)	3.70E+13	0.10	26039.0
F6(7)=ZS(10)+ch3	9.25E+13	-0.07	28702.0
S(32)=S(566)	1.94E+05	2.46	32051.0
S(32)=ZS(6)	4.42E+02	2.96	25145.7
S(566)=c6h10-14d4m+ic3h5co	7.71E+10	0.92	21528.0
S(566)=dipco-24d+c3h5-a	9.45E+13	-0.2	18863
S(566)=ZS(22)+ch3	5.39E+13	0.0	28007
ZS(6)=dipco-24d+c3h5-a	1.28E+17	-0.6	31034
S(305)=ZS(7)+co	3.89E+18	-1.2	16546.1
ZS(7)=ZS(8)	8.19E+07	1.68	26190.0
ZS(7)=ZS(9)	3.06E+03	3.0	29223
ZS(8)=isope+ic4h7	1.27E+12	0.57	29288.7
ZS(9)=isope+ic4h7	1.67E+10	0.85	18770.1
ZS(11)=ZS(12)	3.30E+42	-7.90	42876.0
ZS(12)=ZS(13)	4.52E+11	0.31	23268.0
ZS(13)=c5h6-124d+c3h5-t+co	6.32E+10	-0.25	57568.0

Unimolecular initiation reactions by C–H bond breaking were taken from RMG estimations considering a pressure dependency (rates at 10 atm were considered in this work). Bimolecular initiation steps were also considered and taken from RMG. The formation of biradicals was found to be negligible under our conditions and thus not included.

For hydrogen abstraction reactions by H atoms, presented in Figure 2 (left), and CH_3 radicals, the rate constants calculated by Sirjean et al. (for norbornane) [17] were used as best analogy for the formation of radicals F3 and F4. For radicals F5 and F6, analogies with respect to similar sites in alkanes were considered. For F1 and F2, rate constants proposed by RMG were kept.

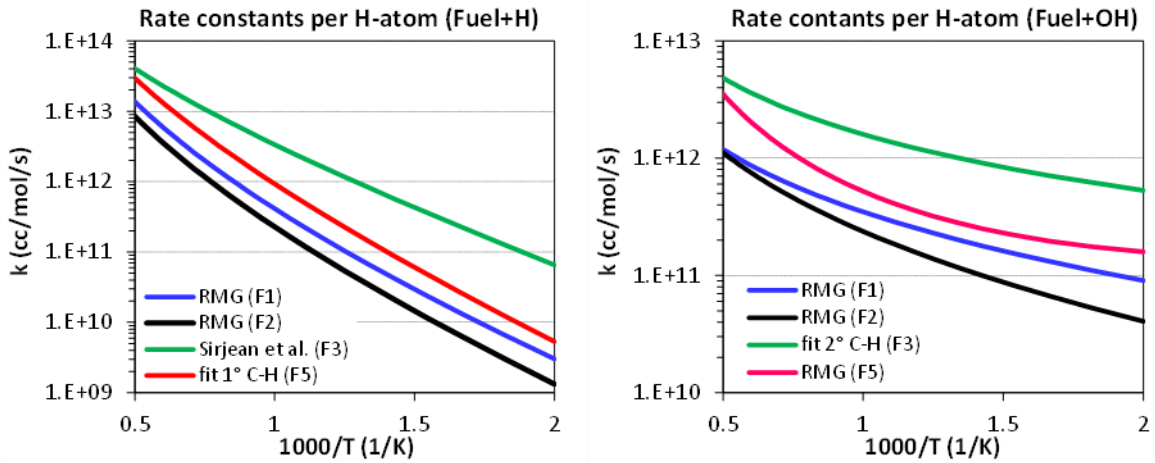

Figure 2. Rate constants for H-abstraction reactions by H (left) and OH (right). F3 and F4 are supposed to have the same rate constants while F6 has twice that of F5.

For H-abstraction reactions by OH radicals, also shown on Figure 2 (right), rate constants suggested by RMG were chosen, except for the F3 and F4 radicals (with bond energies similar to a secondary C–H site in an alkane) where RMG generated rate constants were the same as that for F1 radical. For these secondary C–H sites, rate constants used for alkanes were preferred. These rate constants, referred to as 'fit' in the legend of Figure 2, are typical rate constants that can be used for H-abstraction reactions on alkanes. These are obtained by considering several rate constants from the literature (references to these rate constants and the fits for each C–H site can be found in the Supplementary Material) and fitting them over a wide temperature range.

Rate constants of the beta-scission and internal H-transfer reactions of the fuel radicals, were evaluated using RMG [20]. Once the 6 primary radicals (F1 to F6) decomposed, the rate constants of the reactions involved in the consumption/formation of their products were also taken from RMG online database and used without modifications. The reaction of resonantly stabilized radicals with HO_2, yielding an aldehyde (or a ketone) and a smaller radical, was considered with a rate constant of 4.50×10^{12} mol cm^{-3} s^{-1}.

Thermochemical properties of all species included into our mechanism were evaluated through the group additivity method implemented in RMG [20]. However, it was necessary to revise the estimated thermochemistry for radicals F1, F2, and F3 considering the differences observed on bond dissociation energies with what was expected (see Introduction). Ab initio electronic structure calculations at the CBS-QB3 level of theory implemented in Gaussian 16 [21] and isodesmic reactions were used to get more accurate results in terms of BDEs. The

mechanism file, thermochemistry file, nomenclature and SMILES notations of these species can be obtained from the authors.

4. Results and discussion

This section presents results obtained over a wide range of experimental conditions. Experiments were performed at a constant mean residence time of 0.7s and a constant pressure of 10 atm. Three different equivalence ratios were investigated from fuel-lean to fuel-rich (φ = 0.5, 1, 2). The initial mole fraction of fenchone was set to 1000 ppm for all experiments, and the temperature ranged from 700 to 1180 K.

More than 30 species were detected including alkanes (C_1-C_3), alkenes (C_2-C_5), dienes (C_4-C_6), cyclic olefins, aromatics, and oxygenated compounds. Figure 3 illustrates the evolution of the reactants as a function of the temperature. There, it can be observed that the fuel conversion starts just below 800 K independently of the equivalence ratio. Moreover, the fuel conversion for the fuel-lean mixture appears to be substantially higher than that of the fuel-rich mixture. The developed kinetic mechanism captures well the onset of the reactivity as well as the fuel consumption for the fuel-lean and the stoichiometric mixtures, but predicts a slightly excessive reactivity between 900-1050 K for the fuel-rich mixture.

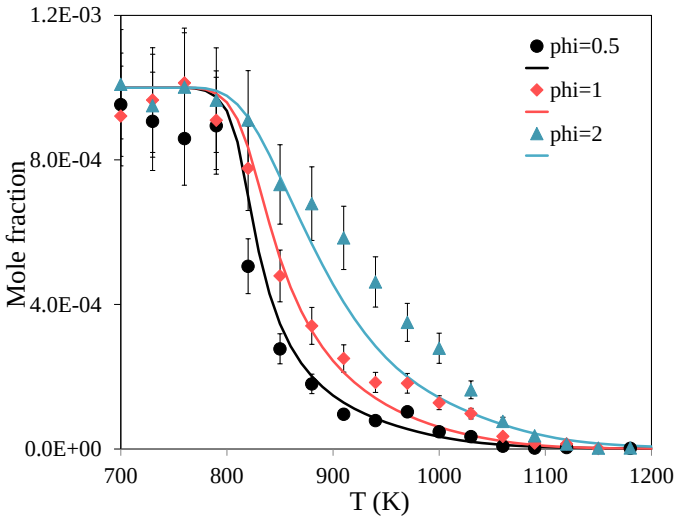

Figure 3. Evolution of the mole fractions of fenchone as a function of temperature for three different equivalence ratios at p = 10 atm, τ = 0.7 s.

The evolution of the mole fractions of the reactants (Fenchone and O_2), and major species is presented in Figure 4. The major intermediate species are CH_4, C_2H_4, and CH_2O, whose maximum mole fractions are 2000 ppm and 1750 ppm, respectively for the rich mixture, whereas formaldehyde is in the order of 180 ppm for all mixtures. As expected, the concentrations of aromatic species increase with the equivalence ratio, the most abundant being benzene. At φ = 2, its mole fraction reaches almost 200 ppm, while it is only 20 ppm at φ = 0.5. Toluene and xylene were also identified in comparable proportions; their mole fractions being maximal for the fuel-rich mixture. Less than 10 ppm of styrene were also detected at φ = 2, and trace amounts in the other conditions. Low quantities of several cyclic species were also observed, such as cyclopentadiene and two different methyl-cyclopentadiene which are formed with similar mole fractions. Finally, among the oxygenated intermediates, acetone, acrolein, methyl vinyl ketone, and methacrolein were also quantified, their mole fractions being higher under fuel-lean conditions.

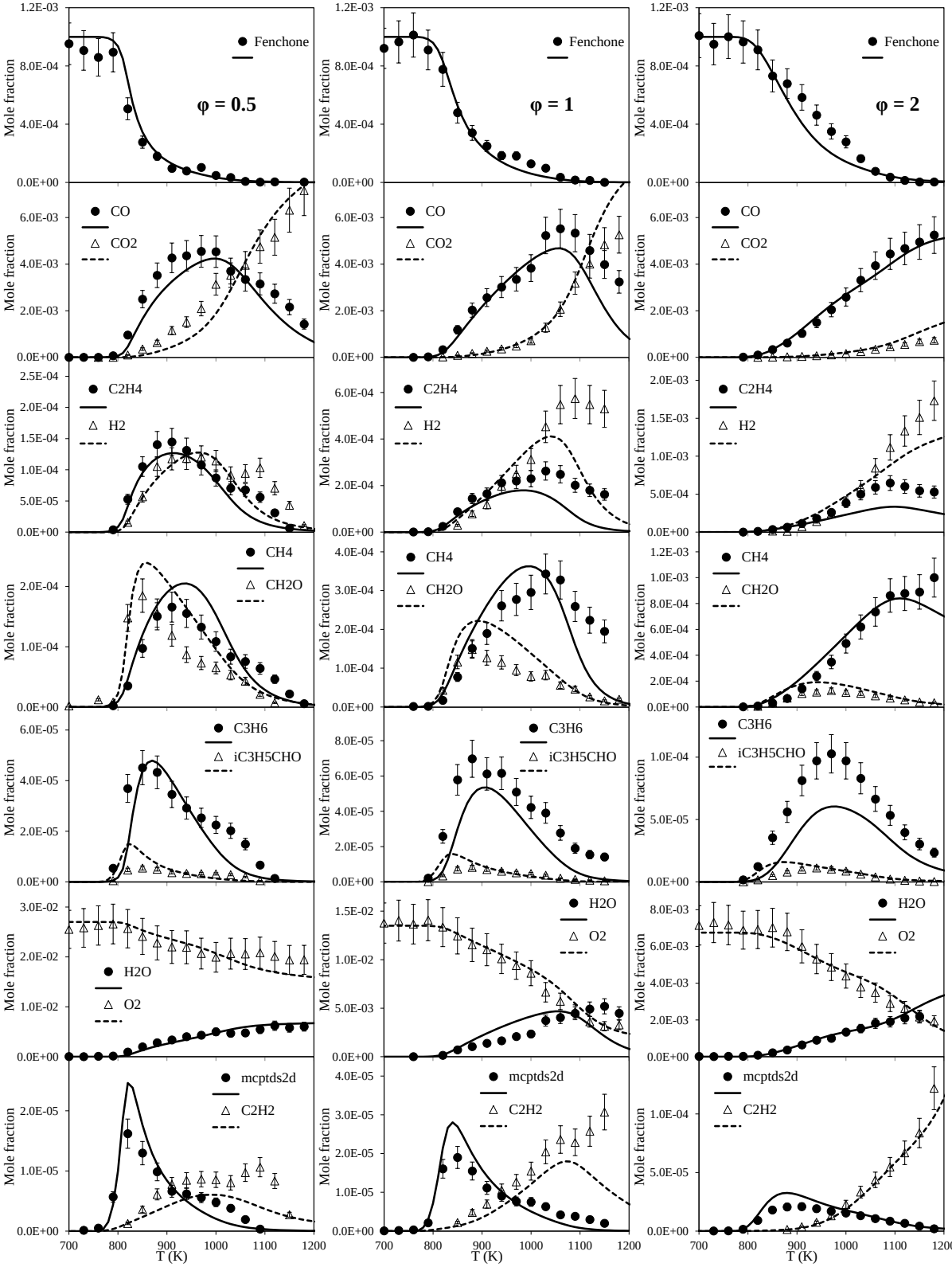

Figure 4. Evolution of the mole fractions of fenchone, O_2, and several stable products as a function of temperature for three different equivalence ratios at p = 10 atm, τ = 0.7 s.

As can be seen from Figure 4, the developed kinetic mechanism captures well the general trend of the fuel consumption as well as the formation and consumption of the different intermediates. Experimentally, it can also be observed that the reactivity slightly decreases (or, at least, does not keep increasing with the temperature) over the temperature range 900-1050

K. This decrease is more and more pronounced when the equivalence ratio increases. It can possibly be attributed to the accumulation of heavy stable intermediates which were not experimentally detected. This decrease in reactivity is not well captured by the model and a more accurate prediction of this phenomenon would constitute a significant improvement of the understanding of the oxidation of fenchone at high temperature. Nevertheless, considering the good agreement observed between calculations and experiments at lower temperature, a reaction pathway analysis was performed under the stoichiometric condition at T = 850 K (temperature at which half of the fenchone is consumed) to unravel the major consumption routes of fenchone under these conditions. The result of this reaction pathways analysis is presented in Figure 5.

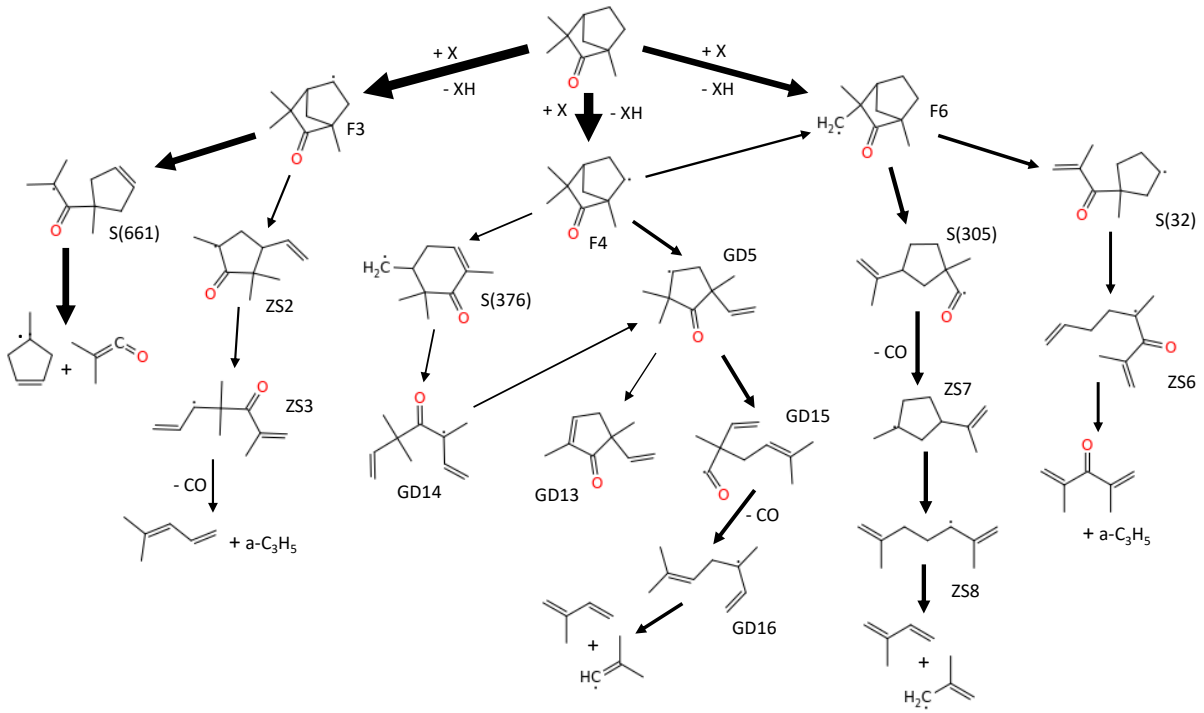

Figure 5. Reaction pathways analysis for the oxidation of fenchone at φ = 1, p = 10 atm, τ = 0.7 s, and T = 850 K. Arrow thickness denotes the intensity of respective carbon flux.

As illustrated by Figure 5, fenchone is mainly consumed by H-abstraction reactions by OH yielding F3 and F4 at the same rate. Though being less produced than F3 and F4 species, F6 is the third most important primary radical in this analysis, F5, F1, and F2 being almost negligible (9%, 5%, and 4% respectively). The fate of F3, F4, and F6 is discussed in the following:

F3- Almost three quarters of F3 decompose into 4-isobutenoxy-4-methyl-1-cyclopentene, S(661), which reacts completely to yield a methyl cyclopentenyl radical and opens the route to benzene (see the next paragraph). The remaining quarter leads to allyl radical and methyl pentadiene, which was not observed experimentally. The third possible C-C β-scission, opening the bridge over the six-membered ring and yielding a radical of a ramified cyclohexanone, appears to be negligible under these conditions.

F4- A quarter of F4 isomerizes into F6, while more than a third produces GD5 (SMILES: C=CC1(C)C[CH]C(C)(C)C(=O)1). The latter is also formed by cyclization of a radical obtained from the 6-membered ring opening. A quarter of GD5 yields a ramified cyclopentenone, the rest produces isoprene and the vinylic isobutenyl radical after ring opening and decarbonylation. This isobutenyl radical is mostly responsible for the formation of acetone. Two other C-C β-scission reactions were considered to consume F4, but it turns out that they are both negligible under these conditions.

F6- The two pathways consuming F6 are similar in terms of flow rate. One yields isoprene after decarbonylation and ring opening, whereas the other one produces diisopropenyl ketone, which was not observed experimentally. A third C-C β-scission was also considered for F6 producing CH_3 radicals, but turns out to be negligible because of its high activation energy resulting from RMG rate rules.

Benzene and subsequent heavier aromatic compounds were found to be produced in significant amounts during the oxidation of fenchone. The particular case of benzene represents a way of possible improvements to better understand the different steps occurring during this process. Figure 6 illustrates how benzene is overestimated by the model under fuel-lean conditions but under estimated at high temperature under fuel-rich conditions. A reaction pathway analysis was performed at φ = 1 and T = 950 K, revealing that benzene is mostly produced by the reactions of methyl cyclopentenyl radicals, methyl cyclopentadienes, methyl cyclopentadienyl radicals, and fulvene. This rate of production analysis is presented in Figure 7 where it can be seen that benzene mostly comes from radical F3 through the formation of methyl cyclopentenyl radicals. Our kinetic mechanism has been significantly modified, in order to account for recent CH_3+C_5H_5 rate constant calculations by Krashnoukov et al. [22], but efforts are still required to better represent benzene accumulation under these conditions, given the diversity of C_6 intermediates and the corresponding benzene formation and consumption pathways [23].

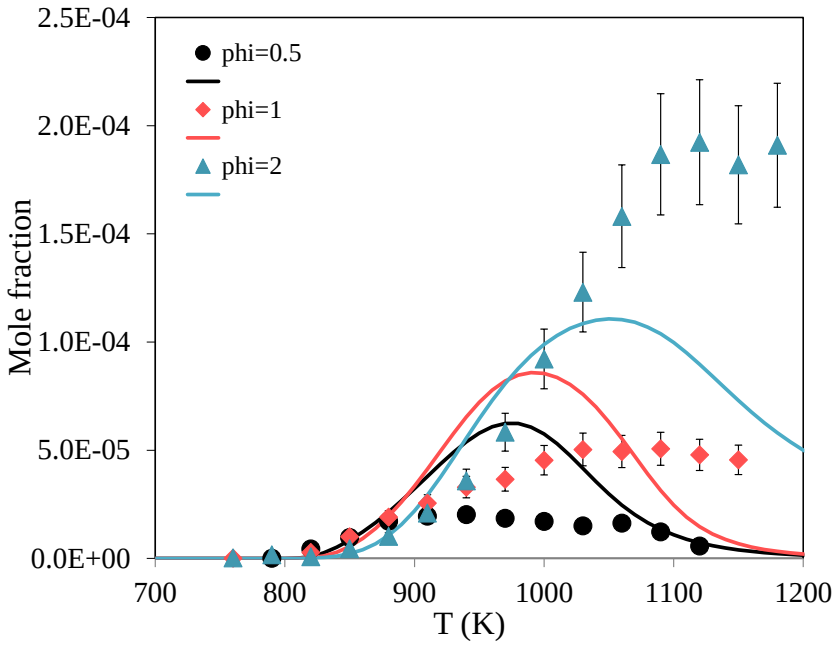

Figure 6. Evolution of the mole fractions of benzene as a function of temperature for three different equivalence ratios at p = 10 atm, τ = 0.7 s.

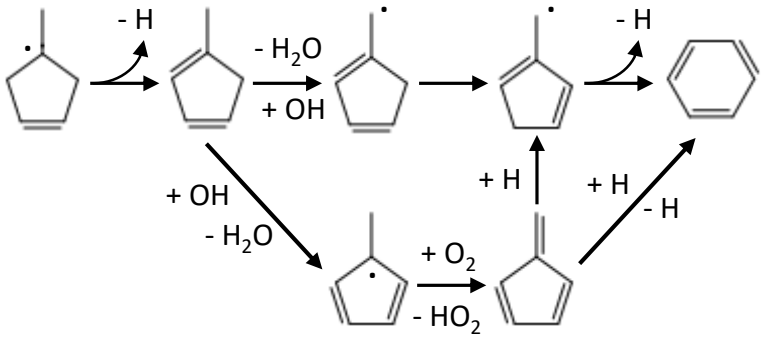

Figure 7. Routes of formation of benzene at p = 10 atm, τ = 0.7 s, and φ = 1.

Conclusions

In the present study, we have investigated the oxidation chemistry of fenchone via detailed speciation experiments in a jet-stirred reactor. Fenchone is a strained-ring hydrocarbon with potentially interesting characteristics (e.g. high energy density) and as a high-octane component however its oxidation chemistry has not been investigated before. A detailed kinetic sub-mechanism of fenchone was developed mostly using the RMG online database and complementary structure/reactivity relations with similar hydrocarbons when available. Three equivalence ratios were chosen for the experiments in order to assess differences in reactivity. The fuel-rich mixture was found to be the least reactive, and is also producing the most important mole fractions of benzene. Reaction pathway analyses showed that benzene formation is closely linked to the chemistry of methyl cyclopentenyl radicals, methyl cyclopentadiene isomers, methyl cyclopentadienyl radicals, and fulvene. These could constitute future targets for model improvement. Apart from benzene, toluene as well as traces of styrene were identified as aromatic products. Among potential oxygenated pollutants, the formation of acrolein and methacrolein was observed. Overall, the kinetic mechanism showed good agreement with the present experimental data and helped us identifying the underlying reaction pathways. Further studies could concern the measurement and modeling of global combustion properties of fenchone in environments close to engine operation such as ignition delay times and flame speeds.

Acknowledgement
Support from the CAPRYSSES project (ANR-11-LABX-006-01) funded by the PIA (Programme d'Investissement d'Avenir) is gratefully acknowledged. The authors thank Aramco Overseas Company for supporting this research.

References

[1] Ausfelder, F., Wagemann, K., "Power-to-Fuels: E-Fuels as an Important Option for a Climate-Friendly Mobility of the Future", *Chem. Ing. Tech.* 92(1-2): 21-30 (2020).
[2] Meylemans, H. A., Quintana, R. L., Harvey, B. G., "Efficient conversion of pure and mixed terpene feedstocks to high density fuels", *Fuel* 97(Supplement C): 560-568 (2012).
[3] Zaabi, A. A., Raj, A., Elkadi, M., Anjum, D., Li, L., George, A., Shebli, M. N. A., "Effects of the addition of a high energy density fuel, adamantane to diesel on its cetane number, sooting propensity, and soot nanostructural properties", *Cleaner Chemical Engineering* 2: 100008 (2022).

[4] Vandewiele, N. M., Magoon, G. R., Van Geem, K. M., Reyniers, M.-F., Green, W. H., Marin, G. B., "Kinetic Modeling of Jet Propellant-10 Pyrolysis", *Energy & Fuels* 29(1): 413-427 (2015).
[5] Abdrabou, M. K., Morajkar, P. P., Guerrero Peña, G. D. J., Raj, A., Elkadi, M., Salkar, A. V., "Effect of 5-membered bicyclic hydrocarbon additives on nanostructural disorder and oxidative reactivity of diffusion flame-generated diesel soot", *Fuel* 275: 117918 (2020).
[6] Salamanca, M., Botero, M. L., Martin, J. W., Dreyer, J. A. H., Akroyd, J., Kraft, M., "The impact of cyclic fuels on the formation and structure of soot", *Combust. Flame* 219: 1-12 (2020).
[7] Andrews, R. J., Smith, C. F., Alexander, A. J., "Mechanism of carbon nanotube growth from camphor and camphor analogs by chemical vapor deposition", *Carbon* 44(2): 341-347 (2006).
[8] Barrientos, E. J., Lapuerta, M., Boehman, A. L., "Group additivity in soot formation for the example of C-5 oxygenated hydrocarbon fuels", *Combust. Flame* 160(8): 1484-1498 (2013).
[9] Morajkar, P. P., Guerrero Peña, G. D. J., Raj, A., Elkadi, M., Rahman, R. K., Salkar, A. V., Pillay, A., Anjana, T., Cha, M. S., "Effects of Camphor Oil Addition to Diesel on the Nanostructures and Oxidative Reactivity of Combustion-Generated Soot", *Energy & Fuels* 33(12): 12852-12864 (2019).
[10] Gao, C. W., Vandeputte, A. G., Yee, N. W., Green, W. H., Bonomi, R. E., Magoon, G. R., Wong, H.-W., Oluwole, O. O., Lewis, D. K., Vandewiele, N. M., Van Geem, K. M., "JP-10 combustion studied with shock tube experiments and modeled with automatic reaction mechanism generation", *Combust. Flame* 162(8): 3115-3129 (2015).
[11] Zhong, B.-j., Zeng, Z.-m., Zhang, H.-z., "An experimental and kinetic modeling study of JP-10 combustion", *Fuel* 312: 122900 (2022).
[12] Parsinejad, F., Arcari, C., Metghalchi, H., "Flame Structure and Burning Speed of JP-10 Air Mixtures", *Combust. Sci. Technol.* 178(5): 975-1000 (2006).
[13] Coudour, B., Chetehouna, K., Courty, L., Garo, J. P., Lemée, L., Mounaïm-Rousselle, C., Halter, F., "Combustion Characteristics of Two Biogenic Volatile Organic Compounds: L-Fenchone and 3-Hexen-1-OL", *Combust. Sci. Technol.* 186(10-11): 1284-1294 (2014).
[14] Courty, L., Chetehouna, K., Halter, F., Foucher, F., Garo, J. P., Mounaïm-Rousselle, C., "Experimental determination of emission and laminar burning speeds of α-pinene", *Combust. Flame* 159(4): 1385-1392 (2012).
[15] Sato, T., Murata, K., Nishimura, A., Tsuchiya, T., Wasada, N., "Pyrolysis of organic compounds—II: The flash pyrolysis of camphor and its related compounds", *Tetrahedron* 23(4): 1791-1798 (1967).
[16] Wang, H., Zhang, B., Gong, S., Wang, L., Zhang, X., Liu, G., "Experimental and modeling studies of quadricyclane and 2-ethylnorbornane pyrolysis from atmospheric to high pressure", *Combust. Flame* 226: 163-181 (2021).
[17] Sirjean, B., Herbinet, O., Glaude, P. A., Ruiz-Lopez, M., Fournet, R., "Theoretical Study of the Thermal Decomposition of a Jet Fuel Surrogate," Proc. WSS/CI Spring 2008 Meeting Paper #08-S11, (2007).
[18] Dagaut, P., Cathonnet, M., Rouan, J. P., Foulatier, R., Quilgars, A., Boettner, J. C., Gaillard, F., James, H., "A jet-stirred reactor for kinetic studies of homogeneous gas-phase reactions at pressures up to ten atmospheres (≈1 MPa)", *Journal of Physics E: Scientific Instruments* 19(3): 207 (1986).
[19] Dayma, G., Thion, S., Serinyel, Z., Dagaut, P., "Experimental and kinetic modeling study of the oxidation of cyclopentane and methylcyclopentane at atmospheric pressure", *Int. J. Chem. Kinet.* 52(12): 943-956

[20] RMG:, https://rmg.mit.edu/.
[21] Frisch, M. J., Trucks, G. W., Schlegel, H. B., Scuseria, G. E., Robb, M. A., Cheeseman, J. R., Scalmani, G., Barone, V., Petersson, G. A., Nakatsuji, H., Li, X., Caricato, M., Marenich, A. V., Bloino, J., Janesko, B. G., Gomperts, R., Mennucci, B., Hratchian, H. P., Ortiz, J. V., Izmaylov, A. F., Sonnenberg, J. L., Williams, Ding, F., Lipparini, F., Egidi, F., Goings, J., Peng, B., Petrone, A., Henderson, T., Ranasinghe, D., Zakrzewski, V. G., Gao, J., Rega, N., Zheng, G., Liang, W., Hada, M., Ehara, M., Toyota, K., Fukuda, R., Hasegawa, J., Ishida, M., Nakajima, T., Honda, Y., Kitao, O., Nakai, H., Vreven, T., Throssell, K., Montgomery Jr., J. A., Peralta, J. E., Ogliaro, F., Bearpark, M. J., Heyd, J. J., Brothers, E. N., Kudin, K. N., Staroverov, V. N., Keith, T. A., Kobayashi, R., Normand, J., Raghavachari, K., Rendell, A. P., Burant, J. C., Iyengar, S. S., Tomasi, J., Cossi, M., Millam, J. M., Klene, M., Adamo, C., Cammi, R., Ochterski, J. W., Martin, R. L., Morokuma, K., Farkas, O., Foresman, J. B., Fox, D. J., "Gaussian 16 Rev. C.01,"Wallingford, CT (2016).
[22] Krasnoukhov, V. S., Porfiriev, D. P., Zavershinskiy, I. P., Azyazov, V. N., Mebel, A. M., "Kinetics of the CH3 + C5H5 Reaction: A Theoretical Study", *The Journal of Physical Chemistry A* 121(48): 9191-9200 (2017).
[23] Hansen, N., Kasper, T., Yang, B., Cool, T. A., Li, W., Westmoreland, P. R., Oßwald, P., Kohse-Höinghaus, K., "Fuel-structure dependence of benzene formation processes in premixed flames fueled by C6H12 isomers", *Proc. Combust. Inst.* 33(1): 585-592 (2011).

Supplementary material

Species nomenclature

Species name	SMILES	Species name	SMILES
fenchone	CC12CCC(C1)C(C)(C)C2=O	ZS(19)	CC12CCC(C1)=C(C)C2=O
F1(1)	CC12CCC([CH]1)C(C)(C)C2=O	ZS(20)	C=C(C)C(=O)C(C)(C)C(=C)[CH2]
F2(11)	CC12CC[C](C1)C(C)(C)C2=O	ZS(21)	O=C=C(C)CCC(=C)[C](C)C
F3(5)	CC12C[CH]C(C1)C(C)(C)C2=O	ZS(23)	C=C(C)CC(=C)[C](C)C
F4(3)	CC12[CH]CC(C1)C(C)(C)C2=O	S(661)	C[C](C)C(=O)C1(C)CC=CC1
F5(9)	O=C1C(C)(C)C2CC1([CH2])CC2	S(32)	C=C(C)C(=O)C1(C)C[CH]CC1
F6(7)	O=C1C([CH2])(C)C2CC1(C)CC2	S(566)	[CH2]C(C)(CC=C)C(=O)C(=C)C
ZS(1)	C1(C)([CH2])C(=O)C(C)(C)C=CC1	dipco-24d	C=C(C)C(=O)C(=C)C
ZS(2)	C=CC1C(C)(C)C(=O)[C](C)C1	dipco-2d4j	C=C(C)C(=O)[C](C)C
ZS(3)	[CH2]C=CC(C)(C)C(=O)C(=C)C	S(305)	C=C(C)C1CCC(C)([C]=O)C1
ZS(5)	C=CC=C(C)C(=O)C(C)=C	S(703)	C=C1CCC(C)=C([O])C1(C)C
ZS(6)	C=CCC[C](C)C(=O)C(=C)C	S(224)	CC(C)=C1CCC(C)([C]=O)C1
ZS(7)	CC(=C)C1CC[C](C)C1	GD(1)	CC1(C)C2CCC(=C2)C(=O)1
ZS(8)	C=C(C)CC[CH]C(=C)C	GD(2)	[CH2]CC1C=C(C)C(=O)C(C)(C)1
ZS(9)	CC(=C)CC([CH2])C(=C)C	GD(3)	[CH2]CC1(C)C=CC(C)(C)C(=O)1
ZS(10)	O=C1C(=C)C2CC1(C)CC2	GD(4)	CC1(C)C(=O)C2=CCC1C2
ZS(11)	O=C1C(=C)C2CC1(C)C[CH]2	GD(5)	C=CC1(C)C[CH]C(C)(C)C(=O)1
ZS(12)	C=CC1C(=C)C(=O)[C](C)C1	GD(6)	CC1=CCC(C1)C(C)(C)[C]=O
ZS(13)	C=C(C)C(=O)C(=C)[CH]C=C	GD(7)	CC1(C)[CH]C=C(C)C(=O)1
ZS(14)	C[C]1CCC(=C(C)C)C1	GD(8)	CC1=CC=C(C)C(=O)1
ZS(15)	C=C(C)CC([CH2])=C(C)C	GD(9)	CC(C)=CC=C(C)[C]=O
ZS(16)	[CH2]C1(C)CC(=C)C(C)(C)C1=O	S(279)	CC1=CC(C(C)(C)[C]=O)CC1
ZS(17)	CC(=C)CC(=C)C(C)(C)[C]=O	S(33)	C=C1CCC(C1)C(C)(C)[C]=O
GD(14)	C=C[C](C)C(=O)C(C)(C)C=C	GD(10)	C[C]=CC=C(C)C
GD(15)	C=CC(C)([C]=O)CC=C(C)C	GD(11)	C[C](C)C1CCC(C)=C1
GD(16)	C=C[C](C)CC=C(C)C	GD(12)	[CH2]CC(C)=CC=C(C)C
GD(17)	C=CC(C)=C=O	GD(13)	C=CC1(C)CC=C(C)C1=O
GD(18)	C[C](C)C1CC=C(C)C1	GD(27)	C=[C]CCC=C
GD(19)	[CH2]C(C)=CCC=C(C)C	C9H15(38)	C=C1CCC(C1)[C](C)C
GD(20)	C=CCC=C(C)C(=O)[C](C)C	C9H15(392)	[CH2]CC(=C)CC=C(C)C
GD(21)	C=CCC=[C]C	C9H15(41)	[CH2]C(=C)CCC=C(C)C
GD(22)	C=[C]CC=C(C)C	S(306)	[CH2]CC1CC(=C)C(=O)C(C)(C)1
GD(23)	[CH2]CC=C(C)C	S(260)	CC1(C)[CH]CC(=C)C(=O)1
GD(24)	[CH2]CC(=C)C(=O)C(C)(C)C=C	C7H8O(583)	C=C1CC=C(C)C1=O
GD(25)	C=[C]C(=O)C(C)(C)C=C	S(582)	CC(C)=CCC(=C)[C]=O
GD(26)	C=CCCC(=C)C(=O)[C](C)C		

Rate constant determination for H-abstraction reactions in alkanes:

Literature is rich in terms of rate constants to be used for H-abstraction reactions from alkanes. These different sources are presented in the following plots and modified Arrhenius fits are obtained from averaging these chosen rate constants. For the sake of space only the most important H-abstraction reactions (by OH and H) in our operating conditions are presented.

H-abstraction by OH radicals:

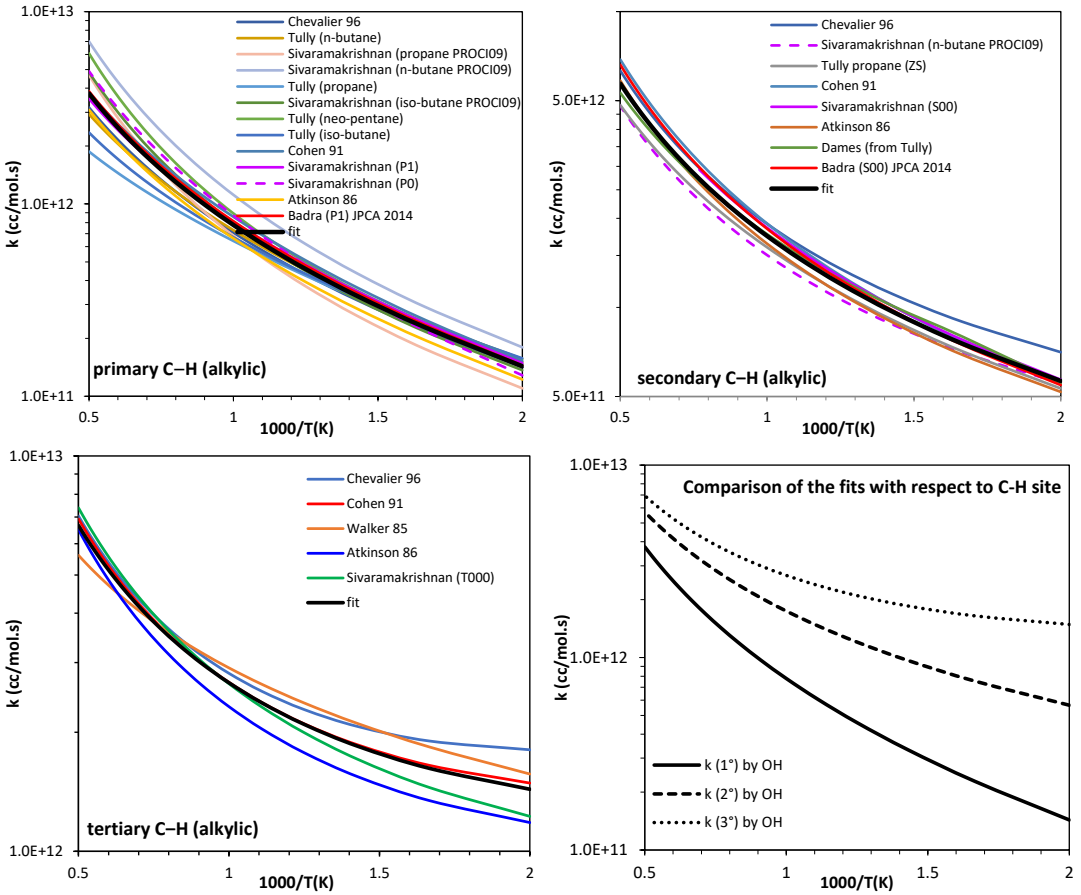

Figure S1. Rate constants of hydrogen abstraction by OH radicals from primary, secondary and tertiary C–H sites in alkanes (per H-atom).

References:

- C. Chevalier, J. Warnatz, H. Melenk, Automatic Generation of Reaction Mechanisms for the Description of the Oxidation of Higher Hydrocarbons, Berichte der Bunsengesellschaft für physikalische Chemie, 94 (1990) 1362-1367.
- F.P. Tully, A.T. Droege, M.L. Koszykowski, C.F. Melius, Hydrogen-atom abstraction from alkanes by hydroxyl. 2. Ethane, The Journal of Physical Chemistry, 90 (1986) 691-698.
- F.P. Tully, J.E.M. Goldsmith, A.T. Droege, Hydrogen atom abstraction from alkanes by hydroxyl. 4. Isobutane, The Journal of Physical Chemistry, 90 (1986) 5932-5937.
- F.P. Tully, M.L. Koszykowski, J. Stephen Binkley, Hydrogen-atom abstraction from alkanes by OH. I. Neopentane and neooctane, Symp. (Int.) Combust., 20 (1985) 715-721.
- A.T. Droege, F.P. Tully, Hydrogen-atom abstraction from alkanes by hydroxyl. 3. Propane, The Journal of Physical Chemistry, 90 (1986) 1949-1954.
- A.T. Droege, F.P. Tully, Hydrogen atom abstraction from alkanes by hydroxyl. 5. n-Butane, The Journal of Physical Chemistry, 90 (1986) 5937-5941.
- R. Sivaramakrishnan, N.K. Srinivasan, M.C. Su, J.V. Michael, High temperature rate constants for OH+ alkanes, Proc. Combust. Inst., 32 (2009) 107-114.
- J.F. Bott, N. Cohen, A shock tube study of the reactions of the hydroxyl radical with several combustion species, Int. J. Chem. Kinet., 23 (1991) 1075-1094.
- R.W. Walker, Temperature coefficients for reactions of OH radicals with alkanes between 300 and 1000 K, Int. J. Chem. Kinet., 17 (1985) 573-582.
- R. Atkinson, Estimations of OH radical rate constants from H-atom abstraction from C–H and O–H bonds over the temperature range 250-1000 K, Int. J. Chem. Kinet., 18 (1986) 555-568.
- J. Badra, E.F. Nasir, A. Farooq, Site-Specific Rate Constant Measurements for Primary and Secondary H- and D-Abstraction by OH Radicals: Propane and n-Butane, The Journal of Physical Chemistry A, 118 (2014) 4652-4660.

H-abstraction by H atoms:

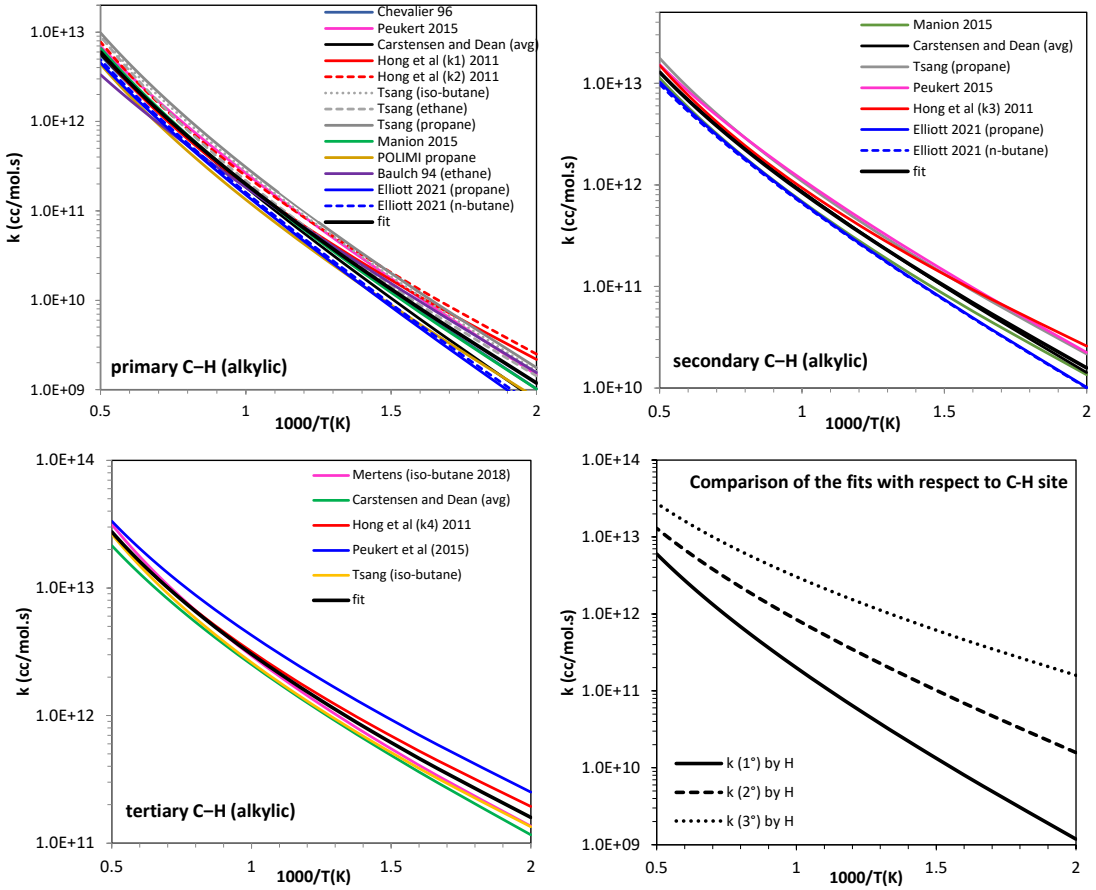

Figure S2. Rate constants of hydrogen abstraction by H atoms from primary, secondary and tertiary C–H sites in alkanes (per H-atom).

References:

- 12) S.L. Peukert, R. Sivaramakrishnan, J.V. Michael, High temperature rate constants for H/D+n-C4H10 and i-C4H10, Proc. Combust. Inst., 35 (2015) 171-179.
- 13) H.-H. Carstensen, A.M. Dean, Rate Constant Rules for the Automated Generation of Gas-Phase Reaction Mechanisms, The Journal of Physical Chemistry A, 113 (2009) 367-380.
- 14) X. Hong, H. Sun, C.K. Law, Rate coefficients of the reactions of isopentane with H and CH3 radicals: Quantum mechanical approach, Computational and Theoretical Chemistry, 963 (2011) 357-364.
- 15) W. Tsang, R.F. Hampson, Chemical Kinetic Data Base for Combustion Chemistry. Part I. Methane and Related Compounds, J. Phys. Chem. Ref. Data, 15 (1986) 1087-1279.
- 16) W. Tsang, Chemical Kinetic Data Base for Combustion Chemistry. Part 3: Propane, J. Phys. Chem. Ref. Data, 17 (1988) 887-951.
- 17) W. Tsang, Chemical Kinetic Data Base for Combustion Chemistry Part 4. Isobutane, J. Phys. Chem. Ref. Data, 19 (1990) 1-68.
- 18) J.A. Manion, D.A. Sheen, I.A. Awan, Evaluated Kinetics of the Reactions of H and CH3 with n-Alkanes: Experiments with n-Butane and a Combustion Model Reaction Network Analysis, The Journal of Physical Chemistry A, 119 (2015) 7637-7658.
- 19) POLIMI propane mechanism : http://creckmodeling.chem.polimi.it/menu-kinetics/menu-kinetics-detailed-mechanisms/107-category-kinetic-mechanisms/399-mechanisms-1911-c1-c3-ht
- 20) D.L. Baulch, C.J. Cobos, R.A. Cox, P. Frank, G. Hayman, T. Just, J.A. Kerr, T. Murrells, M.J. Pilling, J. Troe, R.W. Walker, J. Warnatz, Evaluated Kinetic Data for Combustion Modeling. Supplement I, J. Phys. Chem. Ref. Data, 23 (1994) 847-848.
- 21) S.N. Elliott, K.B. Moore, A.V. Copan, M. Keçeli, C. Cavallotti, Y. Georgievskii, H.F. Schaefer, S.J. Klippenstein, Automated theoretical chemical kinetics: Predicting the kinetics for the initial stages of pyrolysis, Proc. Combust. Inst., 38 (2021) 375-384.
- 22) L.A. Mertens, J.A. Manion, β-Bond Scission and the Yields of H and CH3 in the Decomposition of Isobutyl Radicals, The Journal of Physical Chemistry A, (2018).